Perfect higher-order squeezing via strong nonlinearity in microwave-modified electromagnetically induced transparency

Jun Xu[1] and Fei Wang[2,*]

[1]*College of Physical Science and Technology, Central China Normal University, Wuhan 430079, China*

[2]*College of Science, China Three Gorges University, Yichang 443002, China*

(Received 19 November 2020; revised 21 May 2021; accepted 21 June 2021; published 8 July 2021)

We show that it is possible to obtain perfect higher-order squeezing via strong nonlinearities in the microwave-modified electromagnetically induced transparency (EIT). In a typical Λ three-level system coupled to a control field and a microwave field, the strong nonlinearity is existent under the full-resonant conditions and can be effectively controlled by the relative intensity of the optical and microwave fields. Via dressed-state and Bogoliubov mode transformation, we explore that the internal nonlinearity is closely related to the squeezing parameter and dissipative rate for two cavity modes. As a result, it is found that the two-mode higher-order squeezing is nearly close to 100% under ideal conditions, which is verified by our numerical and analytical results. In addition, we reveal that the higher-order squeezing in the present scheme is robust against the dephasing rate between two lower levels. This may find potential applications in high-precision measurement and provide a convenient way for experimental implementation.

DOI: 10.1103/PhysRevA.104.013706

I. INTRODUCTION

Squeezing is one of the most important issues in the field of quantum optics, quantum information, and nonlinear optics since its wide applications in precision measurements [1–6]. Generally, squeezing is defined with respect to Heisenberg's uncertainty relation. For a pair of quadrature operators, the squeezing occurs when the quantum fluctuations in one quadrature are reduced well below the standard quantum limit, while the other conjugate component increases correspondingly. The theoretical investigation of a squeezed field can be dated back to the 1970s [7] and the experimental observation of the squeezed state was first reported in a Na atomic system based on the nondegenerate four-wave mixing [8]. Since then continuous interest has been paid to study the generation and manipulation of quantum squeezing. The typical schemes include optical parametric processes [9–11], degenerate and nondegenerate four-wave mixing [12–15], stimulated Raman processes [16], and second harmonic generation processes [17].

Successively, the concept of higher-order squeezing was first introduced by Hong and Mandel in 1985 [18]. Hillery proposed another type of higher-order amplitude-squared squeezing of the light field [19,20]. To our knowledge, there exist different types of high-order squeezing and correlations if and only if the uncertainty relation is satisfied. Naturally, the idea of higher-order squeezing can be generalized to a two-mode case in various nonlinear optical systems. For example, Hillery defined one type of two-mode sum squeezing based on a pair of quadrature operators [21]. The sum squeezing is usually generated for two uncorrelated modes if one mode is squeezed while the other one is in a coherent state; otherwise, it is absent if both modes are squeezed. Ansari *et al.* studied the effect of atomic coherence on higher-order squeezing in a two-photon three-level cascade atomic system [22]. In recent years, the theoretical [23–30] and experimental investigation [31–35] of higher-order nonclassicality has attracted extensive attention since it plays a significant role in the high-precision measurement and the detection of gravitational waves. With the so-called Sen-Mandal approach, the dynamical behaviors of higher-order squeezing and higher-order entanglement are discussed in detail in a codirectional nonlinear optical coupler [26], the Bose-Einstein condensates [27], the Raman process [28], four-wave mixing process [29,30] and other systems. Notably, these schemes are mainly focused on the transient higher-order quantum correlations, in which the squeezing and entanglement would disappear gradually in a long enough period due to the saturation effects or environmental noise.

On the other hand, various novel phenomena in electromagnetically induced transparency (EIT) are studied widely based on quantum interference [36–39]. When the light fields are tuned to be subtle away from dark-state resonance, the probe field would experience giant Kerr nonlinearity [40,41], which is the foundation for the high-frequency quantum fluctuations [42–44], quantum memory [39,45–47], and intensity correlation and anticorrelation [48]. Of great interest, the EIT-based systems are reported to be good candidates for the generation of quantum squeezing and entanglement [49–55]. It is demonstrated that quantum entanglement is acquired via the EIT-based nonlinearity [50,51]. A proof-of-principle way is proposed by Yang *et al.* to generate bipartite and multipartite entanglement via spin coherence in EIT [53,54]. More recently, Chuang *et al.* revealed that the coherent population trapping (CPT) nonlinearity can be greatly enhanced by the optical density to directly prepare squeezed light without any

*feiwang@ctgu.edu.cn.

optical cavity [55]. In brief, the nonlinearities in EIT and CPT have great effects on the generation or manipulation of quantum correlations.

Specifically, it was explored that the higher-order single-mode squeezing can be generated in the EIT-based system [56]. By adiabatically eliminating the atomic variables, the exact nonlinear parametric interaction processes are approximately extracted, which can be used to interpret the origin of single-mode higher-order squeezing. However, it is worthwhile to note that there are two main imperfections in the scheme. First, the degree of squeezing, as the order of single-mode squeezed operator increases, is significantly reduced. Second, the steady state higher-order squeezing is hard to realize because the zero frequency squeezing is always absent. To overcome these difficulties, Hu *et al.* utilized atomic reservoir effects, which were first put forward in Pielawa's pioneering work [57], to prepare stable squeezing and entanglement [58–61]. In their work, by applying a pair of strong fields to drive the Λ-type system, the steady-state two-mode squeezing and entanglement were established via two-channel dissipation processes [60,61], in which the best squeezing was enhanced from 50% to nearly 100%. Nevertheless, in these schemes, the good squeezing only existed in a narrow frequency region, and the nonlinear effects were very sensitive to the asymmetrical detunings. This brings forth a challenge in experimental operations. In addition, the EIT-based nonlinearities in realistic systems usually become worse as the dephasing rate between the lower levels deteriorates the atomic coherence, resulting in the reduction of quantum squeezing.

In this paper, we show that the ideal higher-order squeezing is possible to obtain in a Λ-type three-level system driven by a strong control field and a microwave field. Being different from previous schemes [57–61], the strong nonlinearity occurs on the exact resonant conditions and can be conveniently controlled by the relative intensity of the applied fields. This may provide a feasible way to control the degree of squeezing in an experiment. Physically, based on the Bogoliubov mode transformation and adiabatic elimination of atomic variables, we explore that two dissipation channels are formed in the dressed-state picture to generate squeezing. In the reservoir engineering mechanisms, the squeezing parameter, in principle, as the dissipative rate, is closely related to the nonlinear effects in the microwave-modified EIT system. Accordingly, the good squeezing is achieved when the nonlinearity takes a reasonable value. Our analytical and numerical results demonstrate that the stable higher-order squeezing is close to 100% when the relative intensity of the driven fields is near unity. In addition, we show that the perfect higher-order squeezing for the output fields is also possible to obtain. The perfect higher-order squeezing may find potential applications in high-precision measurement and long-distance quantum communications.

The remaining part of the present paper is organized as follows. In Sec. II, we describe the system model that consists of a Λ-type system, a strong coupling field, a strong microwave field, and a weak probe field, and then derive the master equations. The strong nonlinearity in microwave-modified EIT is also analyzed. In Sec. III we present the physical mechanisms and discuss the analytical and numerical results of the two-mode higher-order squeezing for intracavity fields and output fields. Finally, the conclusion is given in Sec. IV.

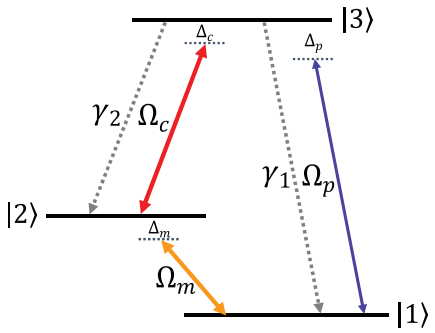

FIG. 1. The level scheme of three-level Λ-type atomic ensemble. The ensemble is driven by a strong control field and a strong microwave field with Rabi frequency Ω_c and Ω_m, and probed by a weak probe field with Rabi frequency Ω_p. The detunings of the atomic frequencies from the corresponding field frequencies are $\Delta_p = \omega_{31} - \omega_p$, $\Delta_c = \omega_{32} - \omega_c$, and $\Delta_m = \omega_{21} - \omega_m$. The three-wave mixing $\omega_p = \omega_c + \omega_m$ is satisfied, and then $\Delta_p = \Delta_c + \Delta_m$.

II. MODEL AND EQUATIONS

Here we consider an atomic ensemble of three-level Λ-type atomic system with two metastable states $|1\rangle$, $|2\rangle$ and one excited state $|3\rangle$. As sketched in Fig. 1, a classical coupled field drives the electric-dipole transition $|3\rangle \leftrightarrow |2\rangle$ and a weak probe field probes the electric-dipole transition $|3\rangle \leftrightarrow |1\rangle$. A microwave field is applied to drive the electric-dipole forbidden atomic transition $|2\rangle \leftrightarrow |1\rangle$ as those in Refs. [62–70]. In the rotating-wave approximation, the Hamiltonian of the system is given as ($\hbar = 1$) [1,2]

$$H_0 = \omega_{21}\sigma_{22} + \omega_{31}\sigma_{33} + [\Omega_p\sigma_{31}e^{-i(\omega_p t - k_p z)} + \Omega_c\sigma_{32}e^{-i(\omega_c t - k_c z)} + \Omega_m\sigma_{21}e^{-i(\omega_m t - k_m z)} + \text{H.c.}], \quad (1)$$

where $\sigma_{lm} = \sum_{\mu=1}^{N} |l_\mu\rangle\langle m_\mu|(l, m = 1, 2, 3)$ are the projection operators of N independent atoms for $l = m$ and the flip operators for $l \neq m$, and $\omega_{j1}(j = 2, 3)$ are atomic transition frequencies. Ω_p, Ω_c, and Ω_m are Rabi frequencies of the probe field, the coupling field, and the microwave field, assumed to be real with frequencies ω_p, ω_c, and ω_m, respectively. k_p, k_c, and k_m are the wave numbers of the corresponding fields. For simplicity, the initial phases of the three fields are assumed to be zero. By making a rotating-wave transformation, we rewrite the system Hamiltonian as

$$H_a = \Delta_m\sigma_{22} + \Delta_p\sigma_{33} + \left[\Omega_c\sigma_{32} + \Omega_p\sigma_{31} + \Omega_m\sigma_{21}^{i(\Delta\omega t - \Delta k z)} + \text{H.c.}\right], \quad (2)$$

where $\Delta_m = \omega_{21} - \omega_m$, $\Delta_p = \omega_{31} - \omega_p$, and $\Delta_c = \omega_{32} - \omega_c$ are the detunings of the atomic frequencies from the corresponding field frequencies. We consider the case in which the three-wave mixing and phase-matching conditions are satisfied, $\Delta\omega = \omega_p - \omega_c - \omega_m = 0$, $\Delta k = k_p - k_c - k_m = 0$, and $\Delta_m = \Delta_p - \Delta_c$. The master equation for the density operator ρ of the atom-field system is given by

$$\dot{\rho} = -i[H_a, \rho] + \mathcal{L}_a\rho \quad (3)$$

with

$$\mathcal{L}_a\rho = \sum_{j=1}^{2}\gamma_j\mathcal{L}_{\sigma_{j3}}\rho + \frac{\gamma_p}{2}\mathcal{L}_{\sigma_p}\rho, \tag{4}$$

herein the first term on the right of Eq. (4) describes the atomic relaxations with rates γ_j from the level $|3\rangle$ to $|j\rangle$ $(j = 1, 2)$, and the second term represents the phase damping between two lower levels with the dephasing rate γ_p, and $\mathcal{L}_o\rho = \frac{1}{2}(2o\rho o^\dagger - o^\dagger o\rho - \rho o^\dagger o)$, $o = \sigma_{13}, \sigma_{23}, \sigma_p = \sigma_{22} - \sigma_{11}$. Then the elements of the density-matrix equations are derived as follows:

$$\begin{aligned}
\dot{\rho}_{31} &= -\Gamma_{31}\rho_{31} + i\Omega_p(\rho_{33} - \rho_{11}) - i\Omega_c\rho_{21} + i\Omega_m\rho_{32},\\
\dot{\rho}_{32} &= -\Gamma_{32}\rho_{32} + i\Omega_c(\rho_{33} - \rho_{22}) - i\Omega_p\rho_{12} + i\Omega_m\rho_{31},\\
\dot{\rho}_{21} &= -\Gamma_{21}\rho_{21} + i\Omega_m(\rho_{22} - \rho_{11}) - i\Omega_c\rho_{31} + i\Omega_p\rho_{23},\\
\dot{\rho}_{33} &= -(\gamma_1 + \gamma_2)\rho_{33} + i\Omega_p(\rho_{31} - \rho_{13}) + i\Omega_c(\rho_{32} - \rho_{23}),\\
\dot{\rho}_{22} &= \gamma_2\rho_{33} + i\Omega_m(\rho_{21} - \rho_{12}) + i\Omega_c(\rho_{23} - \rho_{32}),
\end{aligned} \tag{5}$$

where $\Gamma_{31} = \frac{1}{4}[2(\gamma_1 + \gamma_2) + \gamma_p] + i\Delta_p$, $\Gamma_{32} = \frac{1}{4}[2(\gamma_1 + \gamma_2) + \gamma_p] + i\Delta_c$, and $\Gamma_{21} = \gamma_p + i\Delta_m$. Diagonal elements (ρ_{22}, ρ_{33}) represent level populations and off-diagonal elements $(\rho_{31}, \rho_{32}, \rho_{21})$ represent coherent terms.

As is well known, the response of the atoms to the probe field is described by the susceptibility [1,2]

$$\chi = -\frac{\mu_{13}\rho_{31}}{\varepsilon_0 E_p} \tag{6}$$

with the free space permittivity ε_0 and the electric dipole moment μ_{13}. E_p is the electric field intensity of the probe field and satisfies $\Omega_p = \mu_{13}E_p/\hbar$. The real and imaginary parts of the susceptibility describe the dispersion and the absorption of the atoms, respectively. The ratio of the dispersion to absorption is introduced as the nonlinear parameter [51,59]

$$\eta = \frac{\mathrm{Re}\chi}{\mathrm{Im}\chi}. \tag{7}$$

The absolute value $|\eta|$ of the nonlinear parameter determines the strength of the nonlinearity. The larger the value of $|\eta|$ is, the stronger the nonlinearity will be.

In Fig. 2(a), assuming that the microwave field Ω_m is absent and setting $\Delta_c = 0$, $\Delta_p = \Delta$, we plot the absorption $\mathrm{Im}\chi$ and dispersion $\mathrm{Re}\chi$ in units of $|\mu_{13}|^2/\varepsilon_0$ versus the probe field detuning Δ in units of γ for two cases: $\gamma_p = 0$ (dashed line) and $\gamma_p = 0.01\gamma$ (solid line), in which we define $\gamma_{1,2} = \gamma$. The other parameters are chosen as $\Omega_p = 0.1\gamma$, $\Omega_c = 5\gamma$. The nonlinear parameter η is also plotted as a function of Δ in units of γ in Fig. 2(c). It is obvious that the typical EIT phenomenon is generated for $\gamma_p = 0$ since the value of $\mathrm{Im}\chi$ and $\mathrm{Re}\chi$ are exactly equal to zero ($\mathrm{Im}\chi = \mathrm{Re}\chi = 0$) at $\Delta = 0$. However, when the dephasing rate $\gamma_p \neq 0$, as shown in the insert figure of Fig. 2(a), the exact EIT effect is spoiled due to $\mathrm{Im}\chi \approx 4 \times 10^{-4} \neq 0$. Interestingly, despite the deviation from the zero absorption is subtle, the influence of dephasing rate γ_p on the nonlinearity η is remarkable. From Fig. 2(c), for $\gamma_p = 0$, we find that the strong nonlinearity is increased to infinity ($|\eta| \to \infty$) when the probe detuning is close to zero but it is absent at the exact resonance $\Delta = 0$. Nevertheless, when $\gamma_p = 0.01\gamma$, the nonlinearity first increases to a maximum value 24.7 at $\Delta = \pm 0.49\gamma$ and then decreases to zero at

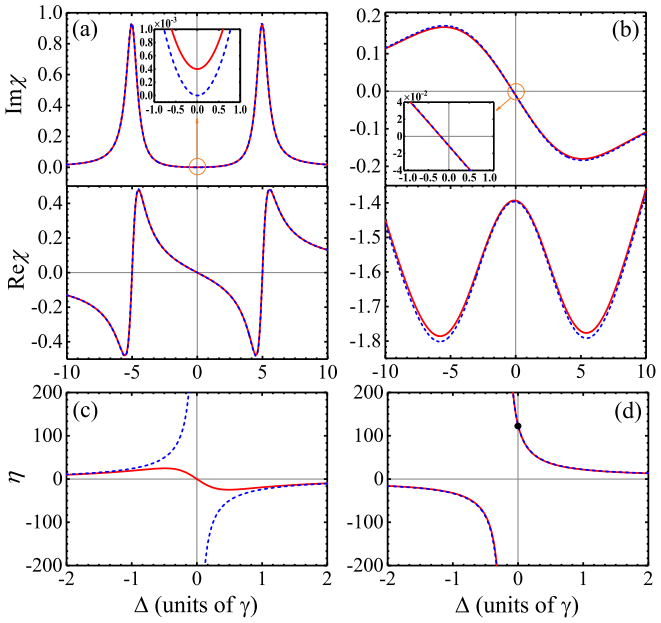

FIG. 2. The absorption $\mathrm{Im}\chi$, the dispersion $\mathrm{Re}\chi$ of the susceptibility in units of $|\mu_{13}|^2/\varepsilon_0$ and the nonlinear parameter $\eta = \mathrm{Re}\chi/\mathrm{Im}\chi$ versus the detuning Δ. (a), (c) $\Omega_m = 0$. (b), (d) $\Omega_m = 5\gamma$. The dashed blue lines denote no dephasing rate. The solid red lines represent the dephasing rate with $\gamma_p = 0.01\gamma$. The black dot in (d) means the nonlinearity at exact resonance. The other parameters are $\gamma_{1,2} = \gamma$, $\Delta_c = 0$, $\Delta_{p,m} = \Delta$, $\Omega_p = 0.1\gamma$, $\Omega_c = 5\gamma$.

$\Delta = 0$. Clearly, the strong nonlinearity is sharply suppressed when the dephasing rate is considered in the realistic atomic system.

As we know, the strong nonlinearity contained in the dark-state system plays an important role in controlling quantum correlations [48–52,59–61]. In these schemes, the asymmetrical detuning is a key factor to modify the nonlinearity, which is responsible for the generation of squeezing and entanglement. However, under the condition of the two-photon resonance, the system will evolve into the dark state, resulting in the disappearance of nonlinearity, quantum squeezing, and quantum entanglement.

Therefore, this motivates us to investigate the appearance of strong nonlinearity under the exact resonant conditions. To do so, we apply a microwave field to couple with the dipole-forbidden transition $|2\rangle \leftrightarrow |1\rangle$ to modify the EIT system [62–70]. As shown by the blue dashed lines in Fig. 2(b), we plot the evolution of absorption and dispersion versus the detuning Δ in units of γ with no dephasing rate by choosing $\Delta_m = \Delta_p = \Delta$ and $\Omega_m = 5\gamma$. The nonlinear parameter η is also shown in Fig. 2(d). Due to $\Delta_c = 0$ and assuming that the Rabi frequencies of the microwave field and control field satisfy $\Omega_c = \Omega_m = \Omega$, the absorption (in units of $|\mu_{13}|^2/\varepsilon_0$) is calculated as

$$\mathrm{Im}\chi = \frac{-\gamma\Omega^2(\Delta + 2\Omega_\mathrm{p})\left(\Omega^2 - \Omega_\mathrm{p}^2 - \Delta\Omega_\mathrm{p}\right)}{\mathrm{G}}, \tag{8}$$

where $G = \Omega_p\Omega^2[\Delta^4 + 3\Delta^2\Omega^2 + 7\Omega^4 + \gamma^2(\Delta^2 + 4\Omega^2)] + \Omega_p^2[5\Delta^2\Omega^2 - 13\Delta^4 + \gamma^2(\Delta^2 + 4\Omega^2)] + 2\Delta\Omega_p\Omega^2(\Delta^2 - 4\Omega^2) + 8\Delta\Omega_p^3\Omega^2 + 5\Omega_p^4\Omega^2 + \Omega_p^6$. Clearly, The probe field

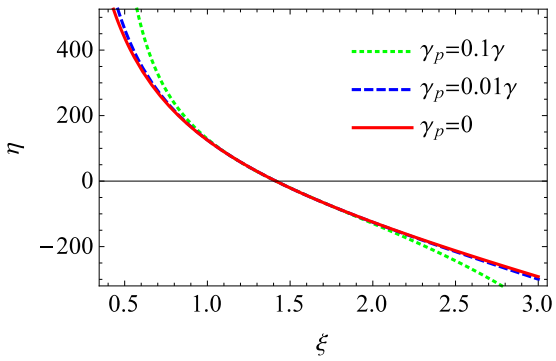

FIG. 3. The nonlinear parameter η at the resonant detuning versus the amplitude ratio ξ for different dephasing rates $\gamma_p = 0.1\gamma$ (dotted line), $\gamma_p = 0.01\gamma$ (dashed line), and $\gamma_p = 0$ (solid line). The other parameters are $\gamma_{1,2} = \gamma$, $\Omega_p = 0.1\gamma$, $\Omega_c = 5\gamma$.

is absorbed in the region of $\Delta < -2\Omega_p(-0.2\gamma)$ while it is amplified when $\Delta > -2\Omega_p(-0.2\gamma)$, which is completely different from the first case in Fig. 2(a). Particularly, at $\Delta = 0$, the absorption value is $\mathrm{Im}\chi = -1.12 \times 10^{-2}$ and the dispersion is $\mathrm{Re}\chi = -1.4$. This indicates that the strong nonlinearity ($\eta = 125$) is obtained at the exact resonant conditions, which is shown in Fig. 2(d) by the black point. In addition, we note that the strong nonlinearities almost remain unchanged when the dephasing rate is $\gamma_p = 0.01$, as shown by the red solid lines in Fig. 2(d), implying that the generated squeezing may be robust against the dephasing rate in the present microwave-modified EIT system. This is sharply different from the exact EIT cases shown in Fig. 2(c).

From now on we only focus on the cases that the driven fields are exactly resonant with the atoms throughout the paper ($\Delta = 0$). Then the analytical expression of η is simplified as

$$\eta = \frac{2\Omega_c\Omega_m^2 - \Omega_p^2\Omega_c - \Omega_c^3}{2\Omega_p\gamma\Omega_m}, \tag{9}$$

herein we take $\gamma_p = 0$. For $\Omega_p \ll \Omega_c$, the nonlinear parameter η can be approximately written as

$$\eta = \frac{\Omega_c^2}{\Omega_p\gamma}\frac{2-\xi^2}{2\xi}, \tag{10}$$

wherein $\xi = \Omega_c/\Omega_m$ is the amplitude ratio of the optical and microwave fields. It is found that the nonlinear effect disappears $\eta = 0$ at the critical point $\xi = \sqrt{2}$. In the region of $0 < \xi < \sqrt{2}$, the strong nonlinearity decreases monotonically, but the absolutely value of $|\eta|$ is increased in the region of $\xi > \sqrt{2}$ as the ratio ξ increases. Despite the analytical expression of the nonlinear parameter including the dephasing rate can be obtained, it is not given here due to its cumbersome expression. In Fig. 3 we plot the numerical dependence of η on ξ for different dephasing rates $\gamma_p = 0.1\gamma$ (dotted line), $\gamma_p = 0.01\gamma$ (dashed line), and $\gamma_p = 0$ (solid line). The other parameters are chosen as $\gamma_{1,2} = \gamma$, $\Omega_p = 0.1\gamma$, $\Omega_c = 5\gamma$. It is found that the phase damping has little influence on the nonlinear effect. In short, the main properties are summarized as follows: (i) the strong nonlinearity is obtained under the exact resonant conditions and can be modified by the relative strength of the applied fields, which may provide great conveniences for experimental implementation; (ii) compared with the conventional EIT-based system, the strong nonlinearity is robust against the dephasing rate, which may be useful for the generation of squeezing and entanglement.

III. PERFECT HIGHER-ORDER SQUEEZING IN MICROWAVE-MODIFIED EIT

In this section, we turn to investigate the physical mechanisms for the two-mode higher-order squeezing in the microwave-modified EIT system. The approximate analytical results and numerical results for two kinds of two-mode fourth-order squeezing are discussed in the following subsection.

A. Analysis of physical mechanisms

We first discuss the internal mechanisms for the generation of two-mode squeezed state in the present microwave-modified EIT system. For the Λ-type atomic system, we apply a control field Ω_c and a microwave field Ω_m to resonantly drive the corresponding transitions $|3\rangle \leftrightarrow |2\rangle$ and $|2\rangle \leftrightarrow |1\rangle$, respectively. Two quantized field modes $a_{1,2}$ are coupled with a common transition $|3\rangle \leftrightarrow |1\rangle$, simultaneously. The possible atomic level structure is plotted in Fig. 4(a). Taking ^{87}Rb atoms as an example, we select $|1\rangle = |5S_{1/2}, F = 1\rangle$, $|2\rangle = |5S_{1/2}, F = 2\rangle$, and $|3\rangle = |5P_{1/2}, F = 2\rangle$. Our scheme may be realized in a geometrical configuration of collinear three wave-mixing as shown in Fig. 4(c). In detail, a Rb cell is installed in a microwave cavity which provides the standing microwave field. Meanwhile, a two-mode cavity ($\mathrm{DCM_1}$-$\mathrm{DCM_2}$) is applied to provide the two-mode fields a_1 and a_2. The cavity fields are combined with the coupling field by a dichroic cavity mirror $\mathrm{DCM_1}$ and then travel through the sample cell and the microwave cavity collinearly with the microwave field. After the microwave cavity, the cavity fields can be filtered by another dichroic cavity mirror $\mathrm{DCM_2}$.

The master equation for the density operator ρ of atom-field interaction system is written in an appropriate rotating frame as

$$\dot{\rho} = -i[H, \rho] + \mathcal{L}_a\rho + \mathcal{L}_c\rho \tag{11}$$

with the total system Hamiltonian

$$H = H_a' + H_I', \tag{12}$$

where

$$H_a' = \Omega_c(\sigma_{32} + \sigma_{23}) + \Omega_m(\sigma_{21} + \sigma_{12}),$$
$$H_I' = \sum_{j=1}^{2} g_j(a_j^\dagger\sigma_{13}e^{-i\delta_j t} + a_j\sigma_{31}e^{i\delta_j t}), \tag{13}$$

where a_j and $a_j^\dagger$ are the annihilation and creation operators for the cavity modes, g_j are the coupling strengths of interactions of the jth cavity fields with the atoms, and $\delta_j = \omega_{31} - \nu_j$ are the detunings of the atomic transition frequency ω_{31} from the cavity field frequencies ν_j ($j = 1, 2$). The cavity loss term $\mathcal{L}_c\rho$ takes the form

$$\mathcal{L}_c\rho = \sum_{j=1}^{2}\kappa_j\mathcal{L}_{a_j}\rho, \tag{14}$$

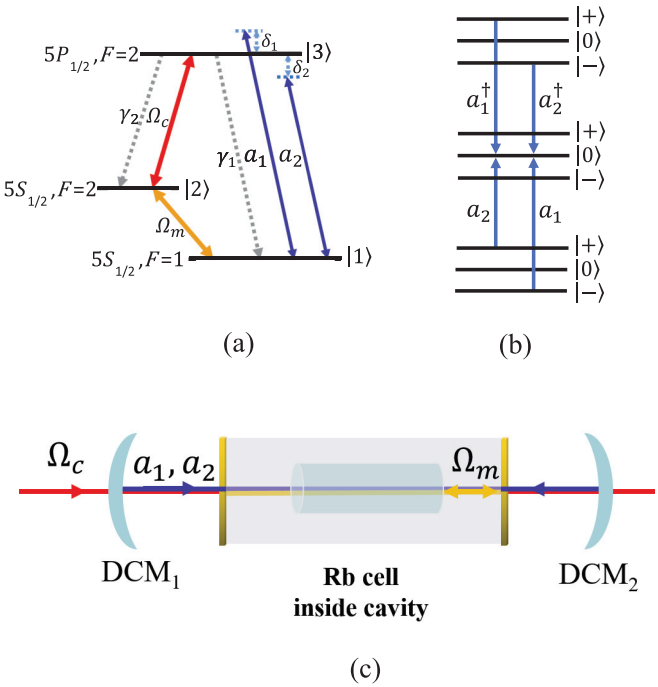

FIG. 4. (a) Configuration with hyperfine levels of ^{87}Rb atoms. The microwave field is coupled resonantly with two hyperfine ground states $5S_{1/2}(F=1)$ and $5S_{1/2}(F=2)$. The coupled field is provided by a diode laser, which is tuned to be resonant at the transition $5S_{1/2}(F=2) \leftrightarrow 5P_{1/2}(F=2)$. Two mode quantum cavity fields are coupled to the transition $5S_{1/2}(F=1) \leftrightarrow 5P_{1/2}(F=2)$. (b) The resonant dressed transitions representation, in which the cavity mode $a_1(a_2)$ is resonant with the sideband $\tilde{\Omega}(-\tilde{\Omega})$, respectively. The dressed atomic transition $|+\rangle$ $(|-\rangle) \rightarrow$ $|0\rangle$ is simultaneously accompanied with creation of one cavity mode a_1 (a_2) and annihilation of the other cavity mode a_2 (a_1). (c) The possible experimental setup for two-mode higher-order squeezing, wherein $DCM_{1,2}$ represent dichroic cavity mirrors, $\Omega_{c,m}$ indicate the control field and microwave field and $a_{1,2}$ are two quantized modes.

where $\mathcal{L}_{a_j}\rho = \frac{1}{2}(2a_j\rho a_j^\dagger - a_j^\dagger a_j\rho - \rho a_j^\dagger a_j)(j=1,2)$, κ_j are the cavity loss rates.

To describe clearly the physical mechanisms and the corresponding conditions for dissipative reservoir effects, we resort to the dressed atomic picture by diagonalizing the Hamiltonian H_a' under the conditions of $\Omega_{c,m} \gg \gamma_j, \kappa_j, g_j(j=1,2)$. The dressed atomic states are expressed in terms of bare states as [4]

$$\begin{aligned} |+\rangle &= \frac{1}{\sqrt{2}}(\cos\theta|1\rangle + |2\rangle + \sin\theta|3\rangle), \\ |0\rangle &= -\sin\theta|1\rangle + \cos\theta|3\rangle, \\ |-\rangle &= \frac{1}{\sqrt{2}}(\cos\theta|1\rangle - |2\rangle + \sin\theta|3\rangle), \end{aligned} \tag{15}$$

with $\cos\theta = \frac{\Omega_m}{\tilde{\Omega}}$, $\sin\theta = \frac{\Omega_c}{\tilde{\Omega}}$, and $\tilde{\Omega} = \sqrt{\Omega_c^2 + \Omega_m^2}$. The dressed states $|0\rangle$, $|+\rangle$, and $|-\rangle$ have their eigenvalues $\lambda_{0,\pm} = 0, \pm\tilde{\Omega}$, respectively. It means that the spacings between these dressed states are identical. Now the free Hamiltonian H_a' becomes the diagonal form in the dressed-state picture

$$H_d = \tilde{\Omega}(\sigma_{++} - \sigma_{--}), \tag{16}$$

and the interaction Hamiltonian H_I' is expressed as

$$\begin{aligned} H_I = &\frac{1}{\sqrt{2}}g_1 a_1^\dagger e^{-i\delta_1 t}(\cos^2\theta\sigma_{+0} - \sin^2\theta\sigma_{0-}) \\ &+ \frac{1}{\sqrt{2}}g_1 a_1^\dagger e^{-i\delta_1 t}(\cos^2\theta\sigma_{-0} - \sin^2\theta\sigma_{0+}) \\ &+ \frac{1}{\sqrt{2}}g_2 a_2 e^{i\delta_2 t}(\cos^2\theta\sigma_{0+} - \sin^2\theta\sigma_{-0}) \\ &+ \frac{1}{\sqrt{2}}g_2 a_2 e^{i\delta_2 t}(\cos^2\theta\sigma_{0-} - \sin^2\theta\sigma_{+0}) \\ &+ \frac{\sin\theta\cos\theta}{2}(g_1 a_1^\dagger e^{-i\delta_1 t} + g_2 a_2 e^{i\delta_2 t}) \\ &\times(\sigma_{+-} + \sigma_{-+} + \sigma_{++} - 2\sigma_{00} + \sigma_{--}) + \text{H.c.}, \end{aligned} \tag{17}$$

where $\sigma_{kl} = \sum_{\mu=1}^{N} |k_\mu\rangle\langle l_\mu|(k,l=0,\pm)$ are the projection operators $(k=l)$ and the flip operators $(k \neq l)$ of the ensemble in terms of the dressed states. Making a further unitary transformation to H_I with $U = \exp(-iH_d t)$, i.e., $UH_I U^\dagger$, choosing Rabi sideband resonance $\delta_1 = -\delta_2 = -\tilde{\Omega}$ and neglecting fast oscillating terms such as $\exp(\pm i\tilde{\Omega}t)$ and $\exp(\pm 2i\tilde{\Omega}t)$ due to the well-separated dressed states $\Omega_{c,m} \gg \gamma_j, \kappa_j$, we retain the second line, the third line, and the corresponding complex conjugate terms in Eq. (17). Then the reduced effective Hamiltonian can be obtained as

$$\begin{aligned} H_{\text{eff}} = &\frac{1}{\sqrt{2}}[\cos^2\theta g_1 a_1 - \sin^2\theta g_2 a_2^\dagger]\sigma_{0-} \\ &+ \frac{1}{\sqrt{2}}[\cos^2\theta g_2 a_2 - \sin^2\theta g_1 a_1^\dagger]\sigma_{0+} + \text{H.c.} \end{aligned} \tag{18}$$

By transforming the bare atomic relaxation terms $\mathcal{L}_a\rho$ into the dressed-state picture according to Eq. (15) and neglecting the quantized modes temporarily, we obtain the steady-state populations $(N_l = \langle\sigma_{ll}\rangle)$ of the dressed states

$$\begin{aligned} N_+ = N_- &= \frac{N(\cos^2\theta + \cos^4\theta)}{1 + 3\cos^4\theta}, \\ N_0 &= \frac{N\sin^4\theta}{1 + 3\cos^4\theta}. \end{aligned} \tag{19}$$

Then the population differences $z = N_+ - N_0 = N_- - N_0$ of the dressed states are derived as follows:

$$z = N_\pm - N_0 = N\frac{2\cos^2\theta - \sin^2\theta}{1 + 3\cos^4\theta}. \tag{20}$$

It is clear that we have $z > 0$ for $0 < \xi < \sqrt{2}$ and $z < 0$ for $\xi > \sqrt{2}$. The dressed atoms as an engineered reservoir will play either a dissipative or amplifying role in different regimes of ξ.

To understand the internal interactions, we further introduce a pair of Bogoliubov modes as $b_1 = a_1\cosh r - a_2^\dagger \sinh r$ and $b_2 = a_2\cosh r - a_1^\dagger \sinh r$ [1,2]. Then the effective interaction Hamiltonian is rewritten as

$$\begin{aligned} H_{\text{eff}} &= g_a(b_1\sigma_{0-} + b_2\sigma_{0+}) + \text{H.c.} \quad \text{for} \quad \xi < 1, \\ H_{\text{eff}} &= g_a(b_1\sigma_{+0} + b_2\sigma_{-0}) + \text{H.c.} \quad \text{for} \quad \xi > 1, \end{aligned} \tag{21}$$

where we have effective coupling constant $g_a = g\sqrt{\frac{1}{2}|\cos(2\theta)|}$ by assuming $g_{1,2} = g$. The squeezing

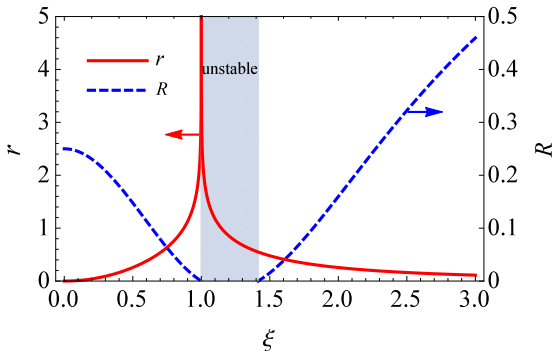

FIG. 5. The squeezing parameter r (solid line) and the dissipation rate R in units of κC (dashed line) versus the amplitude ratio ξ. The changing trends of r and R are completely opposite. The shaded regime shows the unstable region ($1 \leqslant \xi \leqslant \sqrt{2}$). As $\xi \to 1$, $r \to \infty$, and it is possible to obtain a good squeezing. For $\xi \to 0$ or ∞, r is so small that the obtainable squeezing is weak.

parameter r in the two cases is defined through the hyperbolic tangent function as

$$\tanh r = \xi^2 \quad \text{for} \quad \xi < 1,$$
$$\tanh r = \frac{1}{\xi^2} \quad \text{for} \quad \xi > 1. \tag{22}$$

It is seen from the effective Hamiltonian in Eq. (18) that the interactions are established between the quantized modes (a_1, a_2) and the dressed atomic spins $(\sigma_{0+}, \sigma_{0-})$, which is plotted in Fig. 4(b). Clearly, the absorption of mode $a_1(a_2)$ and the creation of modes $a_2(a_1)$ are accompanied by a common dressed transition $|-\rangle \to |0\rangle(|+\rangle \to |0\rangle)$, respectively. Physically, the interactions between two parties a_1 and σ_{0-} (a_2 and σ_{0+}) are referred to as squeezing processes while the other ones between a_2 and $\sigma_{0-}(a_1$ and $\sigma_{0+})$ are named as transferring processes. Accordingly, the two-mode squeezed state of $a_{1,2}$ can be established since the squeezing between a_1 and σ_{0-} is transferred to the mode a_2, i.e., $a_1 \leftrightarrow \sigma_{0-} \curvearrowright a_2$. It is known that the best squeezing degree via such a single chain is about 50% under ideal conditions [57]. Here we can obtain the perfect two-mode squeezing because there exists an alternate chain $a_2 \leftrightarrow \sigma_{0+} \curvearrowright a_1$ [59–61], which is verified by our analytical and numerical results in the following subsection. Essentially, the strong applied fields Ω_c and Ω_m are used to establish atomic reservoir engineering, in which the strong nonlinearity causes the generation of squeezing. We find that the realization of squeezing is strongly dependent on the following two points.

1. Dependence of squeezing parameter r on the nonlinear effects

From Eq. (7), it is seen that the nonlinear parameter η becomes large when the probe field experiences the nonzero dispersion ($\mathrm{Re}\chi \neq 0$) and negligible absorption ($\mathrm{Im}\chi \to 0$). As shown in Figs. 3 and 5, as $\xi \to 0$, we have $\eta \to \infty$ and $r \to 0$. At $\Omega_c = 0$, the atoms would stay in a superposition of ground states $|2\rangle$ and $|1\rangle$. Reasonably, the nonlinear effects disappear since the absorption and dispersion for the probe field are equal to zero. In this case, we can see that the terms of $\sin^2\theta$ in Eq. (18) vanish, giving rise to the absence of transferring processes between $a_1(a_2)$ and $\sigma_{0+}(\sigma_{0-})$. The two-mode squeezed state would not be generated because the two chains are destroyed in this manner, $a_1 \leftrightarrow \sigma_{0-} \nrightarrow a_2$ and $a_2 \leftrightarrow \sigma_{0+} \nrightarrow a_1$. For the other extreme case $\xi \to \infty$, we also have $\eta \to \infty$ and $r \to 0$ when $\Omega_c \gg \Omega_m$. Being different from the first case, the atoms will be entirely trapped into the dark state $|1\rangle$ due to $\Omega_c \gg \Omega_p$ and $\Delta_c = \Delta_p = \Delta = 0$, which is the very case of typical EIT. It is well known that the entanglement and squeezing are impossible to generate since the nonlinear effects disappear on dark-state resonance [50,51,59,60]. From Eq. (18), we find that the squeezing processes are not existent due to $\cos^2\theta \to 0$, which implies that the two above-mentioned chains are spoiled in this way, i.e., $a_1 \nleftrightarrow \sigma_{0-} \curvearrowright a_2$ and $a_2 \nleftrightarrow \sigma_{0+} \curvearrowright a_1$. Specifically, as seen from the strong nonlinear dependence of the squeezing parameter r on the amplitude ratio ξ in Eq. (22), when $\xi \to 1$, we have $r \to \infty$, and then the good squeezing may happen since we have the strong nonlinearity $\eta = 125$ at $\xi = 1$. In a word, the generation of two-mode squeezing is closely related to the nonlinear effects in the present scheme.

2. Analysis of nonlinear dissipative rate

We assume that the atomic variables decay much more rapidly than the cavity modes $\gamma_{1,2} \gg \kappa_{1,2}$. Following the standard quantum optics techniques [1,2], we derive the master equation of the two Bogoliubov modes by adiabatically eliminating the atomic variables by taking the case of $\xi < 1$ as an example

$$\dot{\tilde{\rho}} = \sum_{l=1,2} (A\mathcal{L}_{b_l}\tilde{\rho} + B\mathcal{L}_{b_l^\dagger}\tilde{\rho}) + \mathcal{L}'\tilde{\rho}, \tag{23}$$

where the two Bogoliubov modes $b_{1,2}$ have identical absorption coefficient A and amplification coefficient B,

$$A = \frac{2g_a^2\Gamma N_+}{\Gamma^2 - \gamma_c^2}, \quad B = \frac{2g_a^2\Gamma N_0}{\Gamma^2 - \gamma_c^2}, \tag{24}$$

where $\Gamma = \frac{\gamma}{2}(1 + \cos^2\theta + \sin^2\theta\cos^2\theta)$ and $\gamma_c = -\frac{\gamma}{2}\sin^2\theta\cos^2\theta$ are the decoherence rate of the dressed atoms and the transfer rate of the degenerate dressed transitions, respectively. $\mathcal{L}_{b_l}\tilde{\rho}$ and $\mathcal{L}_{b_l^\dagger}\tilde{\rho}$ have the same form as $\mathcal{L}_{a_j}\tilde{\rho}$ in Eq. (14) and the additional term $\mathcal{L}'\tilde{\rho}$ has the form of

$$\mathcal{L}'\tilde{\rho} = \tilde{C}(b_1\tilde{\rho}b_2 + b_2\tilde{\rho}b_1) - \tilde{D}_1\tilde{\rho}b_1b_2 - \tilde{D}_2b_1b_2\tilde{\rho} + \mathrm{H.c.}, \tag{25}$$

which originates from the coherence transfer between degenerate dressed-state transitions $|+\rangle \rightsquigarrow |0\rangle$ and $|0\rangle \rightsquigarrow |-\rangle$. The parameters are $\tilde{C} = g_a^2N\gamma_c(N_+ + N_0)/(\Gamma^2 - \gamma_c^2)$, $\tilde{D}_1 = 2g_a^2N\gamma_cN_0/(\Gamma^2 - \gamma_c^2)$, $\tilde{D}_2 = 2g_a^2N\gamma_cN_+/(\Gamma^2 - \gamma_c^2)$. Note that $\mathcal{L}'\tilde{\rho}$ is negligibly small because of $(\tilde{C}, \tilde{D}_{1,2}) \ll (A, B)$ ($\gamma_c \ll \Gamma$). Thanks to the dependence of population differences z in Eq. (20) on the parameter ξ, the atomic system leads to either absorption or amplification of Bogoliubov modes $b_{1,2}$. By defining the dissipation rate $R = A - B$, the system is stable when $R > 0$ (absorption is dominant over amplification) while is unstable for $R < 0$ (amplification is dominant over absorption). To observe the nonlinear properties of dissipation rate

R, we analytically solved the dissipation rate as

$$R = \kappa C \frac{(\xi^4 + 4\xi^2 + 2)(\xi^4 - 1)(\xi^2 - 2)}{(\xi^6 + 7\xi^4 + 12\xi^2 + 4)(\xi^4 + 2\xi^2 + 4)}, \quad (26)$$

where the cooperativity parameter $C = 2g^2N/(\kappa\gamma)$ with $\kappa_{1,2} = \kappa$. In Fig. 5, we plot the evolution of squeezing parameter r and dissipation rate R (in units of κC). We note that the evolution of dissipation rate R is divided into three regions. In the regions of $\xi < 1$ and $\xi > \sqrt{2}$, the system is stable for $R > 0$. It implies that the absorption is dominant over amplification, resulting in the possibilities of generated squeezing are confined into the two regions. Nevertheless, in the region of $1 < \xi < \sqrt{2}$ (shown in Fig. 5 by the gray region), the system is unstable since the amplification is dominant over absorption. Thus, the squeezing is impossible to generate in this region. Particularly, at $\xi = 1$, we have $R = 0$ due to the effective coupling constant $g_a = g\sqrt{\frac{1}{2}|\cos^2\theta - \sin^2\theta|} = 0$. Correspondingly, the two-channel interactions of the Bogoliubov modes $b_{1,2}$ in Eq. (21) are no longer existent. When $\xi = \sqrt{2}$, we also have $R = 0$ since the dressed-state populations satisfy the relation $N_\pm = N_0$. In this case, the squeezing is impossible to obtain due to the nonlinearity $\eta = 0$ and dissipation rate $R = 0$ although both the transferring and squeezing processes in Eq. (18) seem to be coexistent.

According to the above analysis, we find that the squeezing parameter r and the dissipative rate R are closely related to the nonlinear effect η. Generally, in the reservoir engineering, good squeezing can be realized when both the squeezing parameter r and the dissipation rate R take large values [57–61]. However, from Fig. 5\, we find that as the ratio ξ increases, the squeezing parameter first increases rapidly to infinity and then drops quickly to zero, while the variation trend of R is inverse. This demonstrates that the two conditions are hard to meet simultaneously. Obviously, good squeezing can be achieved when the squeezing parameter and the dissipation rate have a compatible value.

B. Higher-order squeezing of intracavity fields

As proposed by Hong and Mandel in Ref. [18], a pair of quadrature operators are defined as $X_a = x_{a_1} - x_{a_2}$ and $P_a = p_{a_1} + p_{a_2}$ with the individual operators $x_{a_j} = \frac{1}{\sqrt{2}}(a_j + a_j^\dagger)$, $p_{a_j} = \frac{-i}{\sqrt{2}}(a_j - a_j^\dagger)$ $(j = 1, 2)$. The two-mode fourth-order squeezing occurs if the following inequalities are satisfied:

$$\Delta X_a^4 < 1, \quad \text{or} \quad \Delta P_a^4 < 1. \quad (27)$$

On the other hand, we choose the sum squeezing operator $V_a = \frac{i}{2}(a_1 a_2 - a_1^\dagger a_2^\dagger)$ [21] as the other example to study the four-order squeezing. Similarly, the squeezing is obtainable when

$$\Delta V_N^2 = \frac{\Delta V_a^2}{\tilde{R}} < 1, \quad (28)$$

with a normalized factor $\tilde{R} = \frac{1}{4}(1 + \langle a_1^\dagger a_1\rangle + \langle a_2^\dagger a_2\rangle)$.

It should be pointed out that the quantum fluctuations for Bogoliubov modes $b_{1,2}$ are closely related to the original modes $a_{1,2}$ with the relation of

$$\Delta X_a^4 = e^{-4r}\Delta X_b^4, \quad \Delta P_a^4 = e^{-4r}\Delta P_b^4, \quad (29)$$

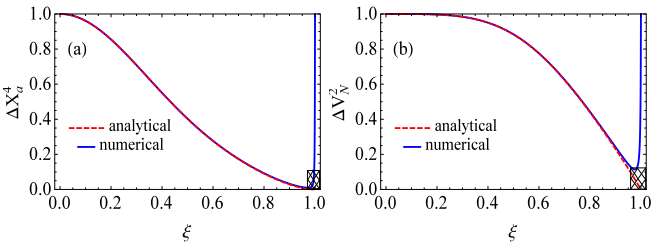

FIG. 6. Analytical (dashed line) and numerical (solid line) results of the normalized variance ΔX_a^4 $(=\Delta P_a^4)$ and ΔV_N^2 versus the amplitude ratio ξ. The analytical results are in very good agreement with the numerical results except for the shadow region near $\xi \to 1$. The parameters of the numerical results are chosen as $\gamma_{1,2} = \gamma$, $\gamma_p = 0$, $\kappa = 0.001\gamma$, $g\sqrt{N} = 1.5\gamma$.

and

$$\Delta V_N^2 = \frac{\Delta V_b^2}{\tilde{R}}, \quad (30)$$

with $V_b = \frac{i}{2}(b_1 b_2 - b_1^\dagger b_2^\dagger)$ and $\tilde{R} = \frac{1}{4}[1 + 2\sinh^2 r + \cosh(2r)(\langle b_1^\dagger b_1\rangle + \langle b_2^\dagger b_2\rangle)]$.

From the reduced density matrix equation in Eq. (23), the analytical results of the steady higher-order moments for Bogoliubov modes can be solved by discarding of the cavity losses temporary. The nonvanishing second-order and fourth-order correlation terms are $\langle b_1^\dagger b_1\rangle = \langle b_2^\dagger b_2\rangle = N_0/(N_+ - N_0)$, $\langle b_1^\dagger b_1^\dagger b_1 b_1\rangle = \langle b_2^\dagger b_2^\dagger b_2 b_2\rangle = 2\langle b_1^\dagger b_1 b_2^\dagger b_2\rangle = 2\langle b_1^\dagger b_1\rangle^2$. Then the normalized variances for the above-mentioned operators are calculated as

$$\Delta X_a^4 = \Delta P_a^4 = e^{-4r}\frac{(N_+ + N_0)^2}{(N_+ - N_0)^2}, \quad (31)$$

and

$$\Delta V_N^2 = \frac{N_+^2 + N_0^2}{4\tilde{R}(N_+ - N_0)^2}. \quad (32)$$

The approximately analytical results of ΔX_a^4 and ΔV_N^2 in the case of $\xi < 1$ are plotted in Fig. 6. We find that the two-mode higher-order squeezing is possible to obtain in a wide region of ξ. Notably, it should be pointed out that the analytical results are only valid when ξ deviates away from $\xi = 1$ appropriately. Since the effective coupling constant g_a and the dissipation rate R are equal to zero at $\xi = 1$, the two-mode squeezing is impossible to generate at this point. Not only that, when ξ is very close to unity, the engineered dissipation is not dominant over the vacuum dissipation. As a consequence, the analytical solution does not hold in a small region around $\xi = 1$, which is depicted by the square shadows in Fig. 6.

To verify the validity of the analytical calculations, we resort to the numerical simulations without discarding the cavity losses $\kappa_{1,2}$. Applying the master equation, we can numerically obtain the results of second-order and fourth-order moments for original cavity modes, which are listed in Appendix B. For simplicity, we define the second-order moments as

$$D_l = \langle a_l^\dagger a_l\rangle, \quad D_3 = \langle a_1 a_2\rangle, \quad D_4 = \langle a_1^\dagger a_2^\dagger\rangle, \quad (33)$$

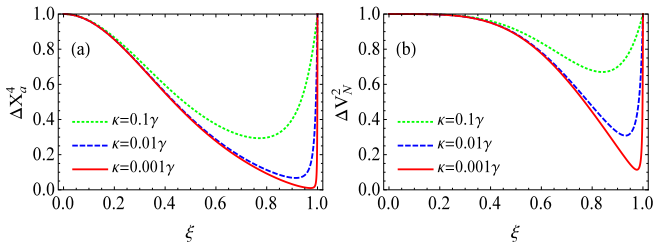

FIG. 7. The normalized variance ΔX_a^4 ($=\Delta P_a^4$) and ΔV_N^2 versus the amplitude ratio ξ for different cavity decay rates $\kappa = 0.1\gamma$ (dotted line), $\kappa = 0.01\gamma$ (dashed line), and $\kappa = 0.001\gamma$ (solid line) by assuming $\kappa_{1,2} = \kappa$. The optimal squeezing of ΔX_a^4 and ΔV_N^2 approaches 100% and 90% below what is for the minimal uncertainty state at $\xi \to 1$. The other parameters are the same as in Fig. 6.

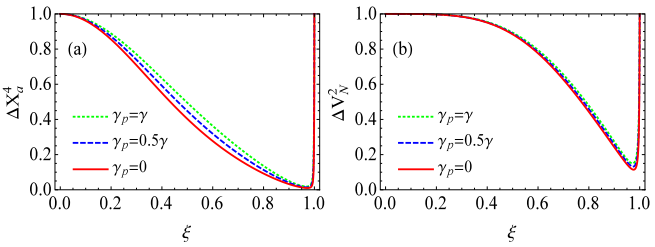

FIG. 8. The normalized variance ΔX_a^4 ($=\Delta P_a^4$) and ΔV_N^2 versus the amplitude ratio ξ for different dephasing rates $\gamma_p = 0$ (solid line), $\gamma_p = 0.5\gamma$ (dashed line), and $\gamma_p = \gamma$ (dotted line). ΔX_a^4 (ΔP_a^4) and ΔV_N^2 are robust against the dephasing rates. We have taken $\kappa = 0.001\gamma$. The other parameters are the same as in Fig. 6.

and the fourth-order moments

$$\begin{aligned} X_l &= \langle a_l^\dagger a_l^\dagger a_l a_l\rangle, \quad X_3 = \langle a_1^\dagger a_1 a_2^\dagger a_2\rangle, \\ Y_1 &= \langle a_1^\dagger a_1 a_1 a_2\rangle, \quad Y_2 = \langle a_1^\dagger a_1^\dagger a_1 a_2^\dagger\rangle, \\ Z_1 &= \langle a_1 a_2^\dagger a_2 a_2\rangle, \quad Z_2 = \langle a_1^\dagger a_2^\dagger a_2^\dagger a_2\rangle, \\ W_1 &= \langle a_1 a_1 a_2 a_2\rangle, \quad W_2 = \langle a_1^\dagger a_1^\dagger a_2^\dagger a_2^\dagger\rangle, \end{aligned} \tag{34}$$

where $l = 1, 2$. The normalized fourth-order squeezing for X_a and P_a are derived as

$$\begin{aligned} \Delta X_a^4 = 1 + 2(D_1 + D_2 - 2D_3) + \tfrac{1}{2}(X_1 + X_2 \\ + 4X_3 + 2W_1 - 4Y_1 - 4Z_1), \end{aligned} \tag{35}$$

and $\Delta P_a^4 = \Delta X_a^4$. We also used the real correlations $D_3 = D_4$, $Y_1 = Y_2$, $W_1 = W_2$, and $Z_1 = Z_2$. Similarly, the sum squeezed operator has its variance

$$\Delta V_N^2 = 1 + \frac{2(X_3 - W_1)}{1 + D_1 + D_2}. \tag{36}$$

From Fig. 6, it is clear that the numerical results are very in agreement with the analytical results except for the shadow region around $\xi = 1$. As the numerical results are strongly dependent on the cavity losses, we plot the fourth-order squeezing ΔX_a^4 and ΔV_N^2 for in Fig. 7 by choosing $\kappa = 0.1$ (dotted line), $\kappa = 0.01$ (dashed line), and $\kappa = 0.001$ (solid line), respectively. With the decreasing of cavity losses, the best squeezing for ΔX_a^4 is changed from 70% at $\xi = 0.77$ to 100% at $\xi = 0.97$ and for ΔV_N^2 is from 30% at $\xi = 0.84$ to 90% at $\xi = 0.98$. This indicates that the perfect higher-order squeezing is obtained in the good cavity limit.

In addition, we showed that the strong nonlinearity is robust against the dephasing rate for the present microwave-modified EIT system in Fig. 3. Reasonably, the two-mode higher-order squeezing may remain stable with the increase of γ_p. In Fig. 8, the normalized variance of ΔX_a^4 and ΔV_N^2 versus the ratio ξ are plotted for different dephasing rates $\gamma_p = 0$ (solid line), $\gamma_p = 0.5\gamma$ (dashed line), and $\gamma_p = \gamma$ (dotted line). Clearly, the variances of two-mode higher-order squeezing ΔX_a^4 and ΔV_N^2 nearly keep unchangeable with the increasing of dephasing rate γ_p. Finally, we should point out that the analytical and numerical results of the higher-order squeezing in the other stable region $\xi > \sqrt{2}$ are also calculated by following the similar procedure. However, we find that the two types of higher-order squeezing are nonexistent since the squeezing parameter r shown in Fig. 5 becomes small.

C. Higher-order squeezing of the output fields

Here we consider the higher-order squeezing of the output fields by defining a pair of EPR-like operators as $X_a^{\rm out} = x_{a_1}^{\rm out} - x_{a_2}^{\rm out}$ and $P_a^{\rm out} = p_{a_1}^{\rm out} + p_{a_2}^{\rm out}$ with the individual operators $x_{a_j}^{\rm out} = \frac{1}{\sqrt{2}}(a_j^{\rm out} + a_j^{\rm out\dagger})$, $p_{a_j}^{\rm out} = \frac{-i}{\sqrt{2}}(a_j^{\rm out} - a_j^{\rm out\dagger})$ ($j = 1, 2$), wherein the operators $a_j^{\rm out}$ represent the output fields. According to the input-output theory $a_j^{\rm out} = a_j^{\rm in} + \sqrt{\kappa_j} a_j$, the quantum correlation of the output fields can be easily obtained. The detailed calculation is presented in Appendix C.

In Fig. 9, the output spectra of $\Delta X_a^4[\omega]$ ($=\Delta P_a^4[\omega]$) and $\Delta V_N^2[\omega]$ are plotted as a function of transformation frequency ω (units of γ). The cavity decay rates and the amplitude ratios in Fig. 9(a) are chosen as $\kappa = 0.1\gamma$, $\xi = 0.82$ (dotted line), $\kappa = 0.05\gamma$, $\xi = 0.89$ (dashed line), $\kappa = 0.01\gamma$, $\xi = 0.973$ (solid line). The cavity decay rates and the amplitude ratios in Fig. 9(b) are chosen as $\kappa = 0.1\gamma$, $\xi = 0.85$ (dotted line), $\kappa = 0.05\gamma$, $\xi = 0.89$ (dashed line), $\kappa = 0.01\gamma$, $\xi = 0.95$ (solid line). The other parameters are the same as in Fig. 6. It is found that the higher-order squeezing spectra are always below the standard quantum limit in a wide frequency domain and the minimal value appears at $\omega = 0$. These results indicate that the perfect higher-order squeezing of the output fields can also be obtained in the present scheme.

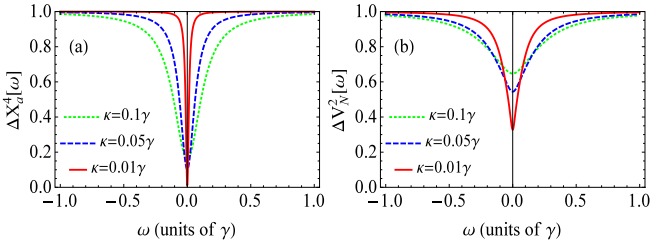

FIG. 9. (a) The output spectra of $\Delta X_a^4[\omega]$ ($=\Delta P_a^4[\omega]$) for $\kappa = 0.1\gamma$, $\xi = 0.82$ (dotted line), $\kappa = 0.05\gamma$, $\xi = 0.89$ (dashed line), $\kappa = 0.01\gamma$, $\xi = 0.973$ (solid line). (b) The output spectra of $\Delta V_N^2[\omega]$ for $\kappa = 0.1\gamma$, $\xi = 0.85$ (dotted line), $\kappa = 0.05\gamma$, $\xi = 0.89$ (dashed line), $\kappa = 0.01\gamma$, $\xi = 0.95$ (solid line). The other parameters are the same as in Fig. 6.

Finally, we would like to stress the differences between the previous schemes and the present microwave-modified EIT system. In conventional EIT-based systems, the generation of squeezing and entanglement is strongly dependent on the asymmetrical detunings of the driven fields [51,54,59–61]. If the two-photon resonance is satisfied, the atoms would be driven into a superposition of two ground states, which is named as a "dark state." In this case, the absorption and dispersion of the atoms are equal to zero, leading to the disappearance of strong nonlinearity. Consequently, quantum entanglement and squeezing are no longer existent. In addition, the EIT-based nonlinear effects usually deteriorate with the increase of the dephasing rate between the lower levels in realistic atomic systems, resulting in the reduction of quantum entanglement and squeezing. However, the main advantages of our scheme are summarized as follows. First, when the applied strong fields are resonant with the transitions, the nonlinearity is obtained and can be modified conveniently by the relative intensity of the two fields. Second, we note that the generated squeezing is robust against the dephasing rate of two lower states. Third, the perfect higher-order squeezing is realized at a steady state by the two-channel squeezing and transferring processes. The internal mechanisms are different from the transient higher-order squeezing in the codirectional nonlinear optical coupler [26], the Bose-Einstein condensates [27], the Raman process [28], and four-wave mixing process [29,30]. In past years, a large number of experimental investigations on higher-order correlations are performed in different quantum optics systems [31–35]. Allevi *et al.* implemented a direct detection scheme of measuring higher-order correlations in the experiment with a pair of hybrid photodetectors [31]. Avenhaus *et al.* experimentally observed the higher-order nonclassicality up to the eighth order with a time-multiplexing detector [32]. Specifically, the higher-order quantum correlations were usually generated based on the nonlinear processes. The perfect higher-order squeezing in the present scheme originates from the microwave-modified strong nonlinearities, which may find potential applications in high-precision measurement and quantum information tasks.

IV. CONCLUSION

In conclusion, we showed that the two-mode fourth-order squeezing can almost approach 90%–100% in the microwave-modified EIT system. When the control field and microwave field are exactly resonant with the atomic system, the strong nonlinearity is generated and can be controlled by the relative intensity of the dressed fields. In the dressed-state picture, it is found that the atomic system acts as a reservoir, by which the perfect higher-order squeezing is achieved at a steady state via two-channel dissipation processes. Since the evolution of the squeezing parameter and the dissipation rate are opposite each other, good squeezing is usually obtainable when the strong nonlinearity takes a proper value. Moreover, we explore that the higher-order squeezing in the present scheme is robust against the dephasing rate between two ground states. This provides a feasible way for experimental realization and may find promising applications in high-precision measurement.

ACKNOWLEDGMENTS

The authors would like to thank Prof. Xiangming Hu and Cheng Gong for their enlightening discussions. This work is supported by the National Natural Science Foundation of China (Grant No. 11574179), and Fundamental Research Funds for the Central Universities (Grant No. CCNU19TS036).

APPENDIX A: REDUCED DENSITY MASTER EQUATION

The reduced master equation in terms of the original $a_{1,2}$ modes in an explicit form

$$\begin{aligned}\dot{\rho}_c =& \alpha_{11}(a_1\rho_c a_1^\dagger - a_1^\dagger a_1\rho_c) + \alpha_{22}(a_1^\dagger\rho_c a_1 - a_1 a_1^\dagger\rho_c)\\ &+ \beta_{11}(a_2\rho_c a_2^\dagger - a_2^\dagger a_2\rho_c) + \beta_{22}(a_2^\dagger\rho_c a_2 - a_2 a_2^\dagger\rho_c)\\ &+ \alpha_{12}(a_2^\dagger\rho_c a_1^\dagger - a_1^\dagger a_2^\dagger\rho_c) + \alpha_{21}(a_1\rho_c a_2 - a_2 a_1\rho_c)\\ &+ \beta_{12}(a_1^\dagger\rho_c a_2^\dagger - a_2^\dagger a_1^\dagger\rho_c) + \beta_{21}(a_2\rho_c a_1 - a_1 a_2\rho_c)\\ &+ \frac{\kappa_1}{2}(a_1\rho_c a_1^\dagger - a_1^\dagger a_1\rho_c) + \frac{\kappa_2}{2}(a_2\rho_c a_2^\dagger - a_2^\dagger a_2\rho_c)\\ &+ \text{H.c.},\end{aligned} \tag{A1}$$

wherein the parameters are given as follows:

$$\begin{aligned}\alpha_{11} =& g_1^2[(\Gamma_2\sin^4\theta - \gamma_{c_1}\sin^2\theta\cos^2\theta)N_0\\ &+ (\Gamma_1\cos^4\theta - \gamma_{c_2}\sin^2\theta\cos^2\theta)N_-]/\Theta,\\ \alpha_{22} =& g_1^2[(\Gamma_2\sin^4\theta - \gamma_{c_1}\sin^2\theta\cos^2\theta)N_+\\ &+ (\Gamma_1\cos^4\theta - \gamma_{c_2}\sin^2\theta\cos^2\theta)N_0]/\Theta,\\ \beta_{11} =& g_2^2[(\Gamma_2\cos^4\theta - \gamma_{c_1}\sin^2\theta\cos^2\theta)N_+\\ &+ (\Gamma_1\sin^4\theta - \gamma_{c_2}\sin^2\theta\cos^2\theta)N_0]/\Theta,\\ \beta_{22} =& g_2^2[(\Gamma_2\cos^4\theta - \gamma_{c_1}\sin^2\theta\cos^2\theta)N_0\\ &+ (\Gamma_1\sin^4\theta - \gamma_{c_2}\sin^2\theta\cos^2\theta)N_-]/\Theta,\\ \alpha_{12} =& g_1 g_2[(\gamma_{c_1}\cos^4\theta - \Gamma_2\sin^2\theta\cos^2\theta)N_0\\ &+ (\gamma_{c_2}\sin^4\theta - \Gamma_1\sin^2\theta\cos^2\theta)N_-]/\Theta,\\ \alpha_{21} =& g_1 g_2[(\gamma_{c_1}\sin^4\theta - \Gamma_2\sin^2\theta\cos^2\theta)N_0\\ &+ (\gamma_{c_2}\cos^4\theta - \Gamma_1\sin^2\theta\cos^2\theta)N_-]/\Theta,\\ \beta_{12} =& g_1 g_2[(\gamma_{c_1}\sin^4\theta - \Gamma_2\sin^2\theta\cos^2\theta)N_+\\ &+ (\gamma_{c_2}\cos^4\theta - \Gamma_1\sin^2\theta\cos^2\theta)N_0]/\Theta,\\ \beta_{21} =& g_1 g_2[(\gamma_{c_1}\cos^4\theta - \Gamma_2\sin^2\theta\cos^2\theta)N_+\\ &+ (\gamma_{c_2}\sin^4\theta - \Gamma_1\sin^2\theta\cos^2\theta)N_0]/\Theta,\end{aligned} \tag{A2}$$

with $\Theta = 2(\Gamma_1\Gamma_2 - \gamma_{c_1}\gamma_{c_2})$, $\Gamma_1 = \gamma_{\rm ph}^{0+} + \frac{1}{4}(\gamma_{\rm ph}^{0-} + \gamma_{\rm ph}^{+-}) + \frac{1}{2}(\gamma_{0+} + \gamma_{+0} + \gamma_{-0} + \gamma_{-+})$, $\Gamma_2 = \gamma_{\rm ph}^{0-} + \frac{1}{4}(\gamma_{\rm ph}^{0+} + \gamma_{\rm ph}^{+-}) + \frac{1}{2}(\gamma_{+0} + \gamma_{0-} + \gamma_{-0} + \gamma_{+-})$; $N_0, N_\pm$ represent the steady-state populations of the dressed states. The damping rates in terms

of the dressed atomic states are

$$\begin{aligned}
\gamma_{0+} &= \gamma_{0-} = \frac{\gamma_1 \sin^4\theta}{2} + \frac{\gamma_p \sin^2 2\theta}{16},\\
\gamma_{+0} &= \gamma_{-0} = \frac{\gamma_1 \cos^4\theta}{2} + \frac{\gamma_2 \cos^2\theta}{2} + \frac{\gamma_p \sin^2 2\theta}{16},\\
\gamma_{+-} &= \gamma_{-+} = \frac{\gamma_1 \sin^2 2\theta}{16} + \frac{\gamma_2 \sin^2\theta}{4} + \frac{\gamma_p(\cos^2\theta+1)^2}{8},\\
\gamma_{\rm ph}^{0+} &= \gamma_{\rm ph}^{0-} = \frac{\gamma_1 \sin^2 2\theta}{4} + \frac{\gamma_p \sin^4\theta}{2},\\
\gamma_{\rm ph}^{+-} &= -\frac{\gamma_1 \sin^2 2\theta}{8} + \frac{\gamma_2 \sin^2\theta}{2} - \frac{\gamma_p \sin^4\theta}{2},\\
\gamma_{c_1} &= \gamma_{c_2} = -\frac{\gamma_1 \sin^2 2\theta}{8} + \frac{\gamma_p \sin^2 2\theta}{16}.
\end{aligned} \tag{A3}$$

APPENDIX B: SECOND-ORDER AND FOURTH-ORDER CORRELATIONS OF TWO INTRACAVITY FIELDS

A closed set of equations for the second-order and fourth-order moments between the modes a_1 and a_2 can be derived from the reduced master equation Eq. (A1) as

$$\begin{aligned}
\frac{d\langle a_1^\dagger a_1\rangle}{dt} &= -2\xi_1\langle a_1^\dagger a_1\rangle + \eta_1(\langle a_1 a_2\rangle + \langle a_1^\dagger a_2^\dagger\rangle) + 2\alpha_{22},\\
\frac{d\langle a_2^\dagger a_2\rangle}{dt} &= -2\xi_2\langle a_2^\dagger a_2\rangle + \eta_2(\langle a_1 a_2\rangle + \langle a_1^\dagger a_2^\dagger\rangle) + 2\beta_{22},\\
\frac{d\langle a_1 a_2\rangle}{dt} &= -\xi_{12}\langle a_1 a_2\rangle + \eta_2\langle a_1^\dagger a_1\rangle + \eta_1\langle a_2^\dagger a_2\rangle - \eta_3,\\
\frac{d\langle a_1^\dagger a_2^\dagger\rangle}{dt} &= -\xi_{12}\langle a_1^\dagger a_2^\dagger\rangle + \eta_2\langle a_1^\dagger a_1\rangle + \eta_1\langle a_2^\dagger a_2\rangle - \eta_3,
\end{aligned} \tag{B1}$$

and

$$\begin{aligned}
\frac{d\langle a_1^\dagger a_1^\dagger a_1 a_1\rangle}{dt} &= -4\xi_1\langle a_1^\dagger a_1^\dagger a_1 a_1\rangle + 2\eta_1(\langle a_1^\dagger a_1 a_1 a_2\rangle\\
&\quad + \langle a_1^\dagger a_1^\dagger a_1 a_2^\dagger\rangle) + 8\alpha_{22}\langle a_1^\dagger a_1\rangle,\\
\frac{d\langle a_2^\dagger a_2^\dagger a_2 a_2\rangle}{dt} &= -4\xi_2\langle a_2^\dagger a_2^\dagger a_2 a_2\rangle + 2\eta_2(\langle a_1 a_2^\dagger a_2 a_2\rangle\\
&\quad + \langle a_1^\dagger a_2^\dagger a_2^\dagger a_2\rangle) + 8\beta_{22}\langle a_2^\dagger a_2\rangle,\\
\frac{d\langle a_1^\dagger a_1 a_2^\dagger a_2\rangle}{dt} &= -2\xi_{12}\langle a_1^\dagger a_1 a_2^\dagger a_2\rangle + \eta_2(\langle a_1^\dagger a_1 a_1 a_2\rangle\\
&\quad + \langle a_1^\dagger a_1^\dagger a_1 a_2^\dagger\rangle) + \eta_1(\langle a_1 a_2^\dagger a_2 a_2\rangle\\
&\quad + \langle a_1^\dagger a_2^\dagger a_2^\dagger a_2\rangle) + 2\beta_{22}\langle a_1^\dagger a_1\rangle + 2\alpha_{22}\langle a_2^\dagger a_2\rangle\\
&\quad - \eta_3(\langle a_1 a_2\rangle + \langle a_1^\dagger a_2^\dagger\rangle),\\
\frac{d\langle a_1^\dagger a_1 a_1 a_2\rangle}{dt} &= -(2\xi_1+\xi_{12})\langle a_1^\dagger a_1 a_1 a_2\rangle + 2\eta_1\langle a_1^\dagger a_1 a_2^\dagger a_2\rangle\\
&\quad + \eta_1\langle a_1 a_1 a_2 a_2\rangle + \eta_2\langle a_1^\dagger a_1^\dagger a_1 a_1\rangle\\
&\quad - 2\eta_3\langle a_1^\dagger a_1\rangle + 4\alpha_{22}\langle a_1 a_2\rangle,\\
\frac{d\langle a_1^\dagger a_1^\dagger a_1^\dagger a_2\rangle}{dt} &= -3(2\xi_1+\xi_{12})\langle a_1^\dagger a_1^\dagger a_1^\dagger a_2\rangle + 3\eta_1\langle a_1^\dagger a_1^\dagger a_1 a_2^\dagger\rangle\\
&\quad + 3\eta_2\langle a_1^\dagger a_1^\dagger a_1^\dagger a_1\rangle - 6\eta_3\langle a_1^\dagger a_1^\dagger\rangle + 12\alpha_{22}\langle a_1^\dagger a_2\rangle,\\
\frac{d\langle a_1 a_2^\dagger a_2 a_2\rangle}{dt} &= -(2\xi_2+\xi_{12})\langle a_1 a_2^\dagger a_2 a_2\rangle + 2\eta_2\langle a_1^\dagger a_1 a_2^\dagger a_2\rangle\\
&\quad + \eta_2\langle a_1 a_1 a_2 a_2\rangle + \eta_1\langle a_2^\dagger a_2^\dagger a_2 a_2\rangle\\
&\quad - 2\eta_3\langle a_2^\dagger a_2\rangle + 4\beta_{22}\langle a_1 a_2\rangle,\\
\frac{d\langle a_1^\dagger a_2^\dagger a_2^\dagger a_2\rangle}{dt} &= -(2\xi_2+\xi_{12})\langle a_1^\dagger a_2^\dagger a_2^\dagger a_2\rangle + 2\eta_2\langle a_1^\dagger a_1 a_2^\dagger a_2\rangle\\
&\quad + \eta_2\langle a_1^\dagger a_1^\dagger a_2^\dagger a_2^\dagger\rangle + \eta_1\langle a_2^\dagger a_2^\dagger a_2 a_2\rangle\\
&\quad - 2\eta_3\langle a_2^\dagger a_2\rangle + 4\beta_{22}\langle a_1^\dagger a_2^\dagger\rangle,\\
\frac{d\langle a_1 a_1 a_2 a_2\rangle}{dt} &= -2\xi_{12}\langle a_1 a_1 a_2 a_2\rangle + 2\eta_2\langle a_1^\dagger a_1 a_1 a_2\rangle\\
&\quad + 2\eta_1\langle a_1 a_2^\dagger a_2 a_2\rangle - 4\eta_3\langle a_1 a_2\rangle,\\
\frac{d\langle a_1^\dagger a_1^\dagger a_2^\dagger a_2^\dagger\rangle}{dt} &= -2\xi_{12}\langle a_1^\dagger a_1^\dagger a_2^\dagger a_2^\dagger\rangle + 2\eta_2\langle a_1^\dagger a_1^\dagger a_1 a_2^\dagger\rangle\\
&\quad + 2\eta_1\langle a_1^\dagger a_2^\dagger a_2^\dagger a_2\rangle - 4\eta_3\langle a_1^\dagger a_2^\dagger\rangle,
\end{aligned} \tag{B2}$$

with $\xi_1 = \alpha_{11} - \alpha_{22} + \frac{\kappa_1}{2}$, $\xi_2 = \beta_{11} - \beta_{22} + \frac{\kappa_2}{2}$, $\xi_{12} = \xi_1 + \xi_2$, $\eta_1 = \beta_{21} - \alpha_{12}$, $\eta_2 = \alpha_{21} - \beta_{12}$, $\eta_3 = \alpha_{12} + \beta_{12}$. By setting $\frac{d}{dt} = 0$, we can solve for the steady-state values for the second-order and fourth-order moments.

APPENDIX C: OUTPUT SECOND-ORDER AND FOURTH-ORDER CORRELATION SPECTRA

The equations of motion for two cavity fields operators can be also derived from the reduced master equation Eq. (A1) as

$$\begin{aligned}
\frac{da_1^\dagger}{dt} &= -\xi_1 a_1^\dagger + \eta_1 a_2 - F_{a_1^\dagger}(t) - \sqrt{\kappa_1}a_1^{\rm in\dagger}(t),\\
\frac{da_2}{dt} &= -\xi_2 a_2 + \eta_2 a_1^\dagger - F_{a_2}(t) - \sqrt{\kappa_2}a_2^{\rm in}(t).
\end{aligned} \tag{C1}$$

Here the input noise operators $a_j^{\rm in}$ satisfy the nonzero correlations $\langle a_j^{\rm in}(t)a_{j'}^{\rm in\dagger}(t')\rangle = \delta_{jj'}\delta(t-t')$. The F's are the zero means noise operators from the atomic reservoir and satisfy the correlations $\langle F_o(t)F_{o'}(t')\rangle = D_{oo'}\delta(t-t')$, where the nonzero diffusion coefficients $D_{a_1a_1^\dagger} = 2\alpha_{11}$, $D_{a_1^\dagger a_1} = 2\alpha_{22}$, $D_{a_2a_2^\dagger} = 2\beta_{11}$, $D_{a_2^\dagger a_2} = 2\beta_{22}$, $D_{a_1a_2} = D_{a_1^\dagger a_2^\dagger} = -\eta_3$.

By performing the Fourier transformation $O(t) = \int_{-\infty}^{\infty} e^{-i\omega t}O[\omega]d\omega/\sqrt{2\pi}$ on Eq. (C1), we have

$$\begin{aligned}
-i\omega a_1^\dagger[-\omega] &= -\xi_1 a_1^\dagger[-\omega] + \eta_1 a_2[\omega] - F_{a_1^\dagger}[-\omega]\\
&\quad - \sqrt{\kappa_1}a_1^{\rm in\dagger}[-\omega],\\
-i\omega a_2[\omega] &= -\xi_2 a_2[\omega] + \eta_2 a_1^\dagger[-\omega] - F_{a_2}[\omega] - \sqrt{\kappa_2}a_2^{\rm in}[\omega].
\end{aligned} \tag{C2}$$

With the input-output relations $a_j^{\rm out}[\omega] = a_j^{\rm in}[\omega] + \sqrt{\kappa_j}a_j[\omega]$, we can express the output fields in terms of the input

ones as

$$\begin{aligned} a_1^{\text{out}}[\omega] &= M_{11}F_{a_1}[\omega] + M_{12}F_{a_2^\dagger}[-\omega] + M_{13}a_1^{\text{in}}[\omega] \\ &\quad + M_{14}a_2^{\text{in}\dagger}[-\omega], \\ a_2^{\text{out}}[\omega] &= M_{21}F_{a_1^\dagger}[-\omega] + M_{22}F_{a_2}[\omega] + M_{23}a_1^{\text{in}\dagger}[-\omega] \\ &\quad + M_{24}a_2^{\text{in}}[\omega], \end{aligned} \tag{C3}$$

where

$$\begin{aligned} M_{11}[\omega] &= \frac{(-i\omega+\xi_2)\sqrt{\kappa_1}}{\eta_1\eta_2+(\omega+i\xi_1)(\omega+i\xi_2)}, \\ M_{12}[\omega] &= \frac{\eta_1\sqrt{\kappa_1}}{\eta_1\eta_2+(\omega+i\xi_1)(\omega+i\xi_2)}, \\ M_{13}[\omega] &= \frac{(-i\omega+\xi_2)\kappa_1+\eta_1\eta_2+(\omega+i\xi_1)(\omega+i\xi_2)}{\eta_1\eta_2+(\omega+i\xi_1)(\omega+i\xi_2)}, \\ M_{14}[\omega] &= \frac{\eta_1\sqrt{\kappa_1\kappa_2}}{\eta_1\eta_2+(\omega+i\xi_1)(\omega+i\xi_2)}, \\ M_{21}[\omega] &= \frac{\eta_2\sqrt{\kappa_2}}{\eta_1\eta_2+(\omega+i\xi_1)(\omega+i\xi_2)}, \\ M_{22}[\omega] &= \frac{(-i\omega+\xi_1)\sqrt{\kappa_2}}{\eta_1\eta_2+(\omega+i\xi_1)(\omega+i\xi_2)}, \\ M_{23}[\omega] &= \frac{\eta_2\sqrt{\kappa_1\kappa_2}}{\eta_1\eta_2+(\omega+i\xi_1)(\omega+i\xi_2)}, \\ M_{24}[\omega] &= \frac{(-i\omega+\xi_1)\kappa_2+\eta_1\eta_2+(\omega+i\xi_1)(\omega+i\xi_2)}{\eta_1\eta_2+(\omega+i\xi_1)(\omega+i\xi_2)}. \end{aligned} \tag{C4}$$

The second-order correlation spectra can be obtained as follows:

$$\begin{aligned} &\langle a_1^{\text{out}\dagger}[-\omega]a_1^{\text{out}}[\omega]\rangle \\ &= |M_{11}[-\omega]|^2 D_{a_1^\dagger a_1} + |M_{12}[-\omega]|^2 D_{a_2 a_2^\dagger} \\ &\quad + (M_{12}[-\omega])^* M_{11}[-\omega] D_{a_1 a_2} \\ &\quad + (M_{11}[-\omega])^* M_{12}[-\omega] D_{a_1^\dagger a_2^\dagger} + |M_{14}[-\omega]|^2, \\ &\langle a_2^{\text{out}\dagger}[-\omega]a_2^{\text{out}}[\omega]\rangle \\ &= |M_{21}[-\omega]|^2 D_{a_1 a_1^\dagger} + |M_{22}[-\omega]|^2 D_{a_2^\dagger a_2} \\ &\quad + (M_{21}[-\omega])^* M_{22}[-\omega] D_{a_1 a_2} \\ &\quad + (M_{22}[-\omega])^* M_{21}[-\omega] D_{a_1^\dagger a_2^\dagger} + |M_{23}[-\omega]|^2, \\ &\langle a_1^{\text{out}}[\omega]a_2^{\text{out}}[\omega]\rangle \\ &= M_{11}[\omega]M_{21}[-\omega] D_{a_1 a_1^\dagger} + M_{12}[\omega]M_{22}[-\omega] D_{a_2^\dagger a_2} \\ &\quad + M_{11}[\omega]M_{22}[-\omega] D_{a_1 a_2} + M_{12}[\omega]M_{21}[-\omega] D_{a_1^\dagger a_2^\dagger} \\ &\quad + M_{13}[\omega]M_{23}[-\omega]. \end{aligned} \tag{C5}$$

By performing the Fourier transformation on Eq. (B2), we can obtain the fourth-order correlation spectra $X_k[\omega], Y_j[\omega], Z_j[\omega], W_j[\omega] (k = 1-3,\ j = 1, 2)$, respectively. The output spectra of $\Delta X_a^4[\omega]$ $(=\Delta P_a^4[\omega])$ and $\Delta V_N^2[\omega]$ can be derived from the second-order and fourth-order correlation spectra.

[1] D. F. Walls and G. J. Milburn, *Quantum Optics* (Springer-Verlag, Berlin, 1994).
[2] M. O. Scully and M. S. Zubairy, *Quantum Optics* (Cambridge University Press, Cambridge, England, 1997).
[3] R. W. Boyd, *Nonlinear Optics 3rd ed.* (Academic, New York, 2008).
[4] C. Cohen-Tannoudji, J. Dupont-Roc, and G. Grynberg, *Atom-Photon Interactions* (Wiley, New York, 1992).
[5] P. Meystre and M. Sargent, III, *Elements of Quantum Optics* (Springer, New York, 2007).
[6] R. Loudon and P. L. Knight, J. Mod. Opt. **34**, 709 (1987).
[7] D. Stoler, Phys. Rev. D **1**, 3217 (1970).
[8] R. E. Slusher, L. W. Hollberg, B. Yurke, J. C. Mertz, and J. F. Valley, Phys. Rev. Lett. **55**, 2409 (1985).
[9] L. A. Wu, H. J. Kimble, J. L. Hall, and H. F. Wu, Phys. Rev. Lett. **57**, 2520 (1986).
[10] Z. Y. Ou, S. F. Pereira, H. J. Kimble, and K. C. Peng, Phys. Rev. Lett. **68**, 3663 (1992).
[11] Y. Zhang, H. Wang, X. Y. Li, J. T. Jing, C. D. Xie, and K. C. Peng, Phys. Rev. A **62**, 023813 (2000).
[12] R. S. Bondurant, P. Kumar, J. H. Shapiro, and M. Maeda, Phys. Rev. A **30**, 343 (1984).
[13] M. D. Reid, D. F. Walls, and B. J. Dalton, Phys. Rev. Lett. **55**, 1288 (1985).
[14] R. Guzmán, J. C. Retamal, E. Solano, and N. Zagury, Phys. Rev. Lett. **96**, 010502 (2006).
[15] R. M. Shelby, M. D. Levenson, S. H. Perlmutter, R. G. De Voe, and D. F. Walls, Phys. Rev. Lett. **57**, 691 (1986).
[16] J. Perina, *Quantum Statistics of Linear and Nonlinear Optical Phenomena* (Kluwer, Amsterdam, 1991).
[17] L. Mandel, Opt. Commun. **42**, 437 (1982).
[18] C. K. Hong and L. Mandel, Phys. Rev. Lett. **54**, 323 (1985).
[19] M. Hillery, Opt. Commun. **62**, 135 (1987).
[20] M. Hillery, Phys. Rev. A **36**, 3796 (1987).
[21] M. Hillery, Phys. Rev. A **40**, 3147 (1989).
[22] N. A. Ansari and M. S. Zubairy, Phys. Rev. A **44**, 2214 (1991); N. A. Ansari, *ibid.* **48**, 4686 (1993).
[23] M. H. Mahran, Phys. Rev. A **45**, 5113 (1992).
[24] A. V. Chizhov, J. W. Haus, and K. C. Yeong, Phys. Rev. A **52**, 1698 (1995).
[25] G. S Agarwal and A. Biswas, New J. Phys. **7**, 211 (2005).
[26] K. Thapliyal, A. Pathak, B. Sen, and J. Peřina, Phys. Rev. A **90**, 013808 (2014).
[27] S. K. Giri, B. Sen, C. H. Raymond Ooi, and A. Pathak, Phys. Rev. A **89**, 033628 (2014).
[28] S. K. Giri, B. Sen, A. Pathak, and P. C. Jana, Phys. Rev. A **93**, 012340 (2016).
[29] M. Das, B. Sen, A. Ray, and A. Pathak, Ann. Phys. (Leipzig) **530**, 1700160 (2018).
[30] J. J. Gong and P. K. Aravind, Phys. Rev. A **46**, 1586 (1992).
[31] A. Allevi, S. Olivares, and M. Bondani, Phys. Rev. A **85**, 063835 (2012).
[32] M. Avenhaus, K. Laiho, M. V. Chekhova, and C. Silberhorn, Phys. Rev. Lett. **104**, 063602 (2010).
[33] J. Peřina, Jr., V. Michálek, and O. Haderka, Phys. Rev. A **96**, 033852 (2017).

[34] E. E. Rowen, N. Bar-Gill, and N. Davidson, Phys. Rev. Lett. **101**, 010404 (2008).
[35] C. M. Li, K. Chen, A. Reingruber, Y. N. Chen, and J. W. Pan, Phys. Rev. Lett. **105**, 210504 (2010).
[36] S. E. Harris, Phys. Today **50(7)**, 36 (1997).
[37] J. P. Marangos, J. Mod. Opt. **45**, 471 (1998).
[38] M. D. Lukin, Rev. Mod. Phys. **75**, 457 (2003).
[39] M. Fleischhauer, A. Imamoglu, and J. P. Marangos, Rev. Mod. Phys. **77**, 633 (2005).
[40] S. J. Li, X. D. Yang, X. M. Cao, C. H. Zhang, C. D. Xie, and H. Wang, Phys. Rev. Lett. **101**, 073602 (2008).
[41] G. Dmochowski, A. Feizpour, M. Hallaji, C. Zhuang, A. Hayat, and A. M. Steinberg, Phys. Rev. Lett. **116**, 173002 (2016).
[42] M. Fleischhauer, Phys. Rev. Lett. **72**, 989 (1994).
[43] P. Barberis-Blostein and M. Bienert, Phys. Rev. Lett. **98**, 033602 (2007).
[44] J. A. Souza, E. Figueroa, H. Chibani, C. J. Villas-Boas, and G. Rempe, Phys. Rev. Lett. **111**, 113602 (2013).
[45] M. T. L. Hsu, G. Hétet, O. Glöckl, J. J. Longdell, B. C. Buchler, H. A. Bachor, and P. K. Lam, Phys. Rev. Lett. **97**, 183601 (2006).
[46] G. Heinze, C. Hubrich, and T. Halfmann, Phys. Rev. Lett. **111**, 033601 (2013).
[47] Y. F. Hsiao, P. J. Tsai, H. S. Chen, S. X. Lin, C. C. Hung, C. H. Lee, Y. H. Chen, Y. F. Chen, I. A. Yu, and Y. C. Chen, Phys. Rev. Lett. **120**, 183602 (2018).
[48] V. A. Sautenkov, Y. V. Rostovtsev, and M. O. Scully, Phys. Rev. A **72**, 065801 (2005).
[49] P. Barberis-Blostein and N. Zagury, Phys. Rev. A **70**, 053827 (2004).
[50] V. Josse, A. Dantan, L. Vernac, A. Bramati, M. Pinard, and E. Giacobino, Phys. Rev. Lett. **91**, 103601 (2003).
[51] A. Dantan, J. Cviklinski, E. Giacobino, and M. Pinard, Phys. Rev. Lett. **97**, 023605 (2006).
[52] A. Sinatra, Phys. Rev. Lett. **97**, 253601 (2006).
[53] X. Yang, J. Sheng, U. Khadka, and M. Xiao, Phys. Rev. A **85**, 013824 (2012); X. Yang, Y. Zhou, and M. Xiao, *ibid.* **85**, 052307 (2012).
[54] X. Yang, Y. Zhou, and M. Xiao, Sci. Rep. **3**, 3479 (2013); X. Yang and M. Xiao, *ibid.* **5**, 13609 (2015); X. Yang, J. Shang, B. Xue, Y. Zhou, and M. Xiao, Opt. Express **22**, 12563 (2014).
[55] Y. L. Chuang, R. K. Lee, and I. A. Yu, Phys. Rev. A **91**, 063818 (2015); Y. L. Chuang, I. A. Yu, and R. K. Lee, *ibid.* **96**, 053818 (2017).
[56] F. Wang and X. M. Hu, Europhys. Lett. **108**, 54007 (2014).
[57] S. Pielawa, G. Morigi, D. Vitali, and L. Davidovich, Phys. Rev. Lett. **98**, 240401 (2007).
[58] F. Wang, W. Nie, and C. H. Oh, J. Opt. Soc. Am. B **34**, 130 (2017); F. Wang, W. Nie, X. L. Feng, and C. H. Oh, Phys. Rev. A **94**, 012330 (2016).
[59] X. M. Hu, Q. P. Hu, L. C. Li, C. Huang, and S. Rao, Phys. Rev. A **96**, 063824 (2017).
[60] X. M. Hu, Phys. Rev. A **92**, 022329 (2015); G. L. Cheng, X. M. Hu, W. X. Zhong, and Q. Li, **78**, 033811 (2008).
[61] W. Wang, X. M. Hu, and J. Xu, Opt. Exp. **27**, 30530 (2019).
[62] M. P. Winters, J. L. Hall, and P. E. Toschek, Phys. Rev. Lett. **65**, 3116 (1990).
[63] H. Li, V. A. Sautenkov, Y. V. Rostovtsev, G. R. Welch, P. R. Hemmer, and M. O. Scully, Phys. Rev. A **80**, 023820 (2009).
[64] A. Karigowda, A. K V, P. K. Nayak, S. Sudha, B. C. Sanders, F. Bretenaker, and A. Narayanan, Opt. Express **27**, 32111 (2019).
[65] X. J. Zhang, Z. H. Shi, H. H. Wang, Z. H. Kang, and J. H. Wu, Phys. Rev. A **99**, 033817 (2019).
[66] E. A. Wilson, N. B. Manson, C. Wei, and L. Yang, Phys. Rev. A **72**, 063813 (2005); E. A. Wilson, N. B. Manson, and C. Wei, *ibid.* **72**, 063814 (2005).
[67] N. Radwell, T. W. Clark, B. Piccirillo, S. M. Barnett, and S. Franke-Arnold, Phys. Rev. Lett. **114**, 123603 (2015).
[68] S. Sharma and T. N. Dey, Phys. Rev. A **96**, 033811 (2017).
[69] Rajitha K. V. and T. N. Dey, Phys. Rev. A **94**, 053851 (2016).
[70] A. Jagannathan, N. Arunkumar, J. A. Joseph, and J. E. Thomas, Phys. Rev. Lett. **116**, 075301 (2016).